ACS APPLIED MATERIALS & INTERFACES

Research Article

www.acsami.org

Microgrooved Polymer Substrates Promote Collective Cell Migration To Accelerate Fracture Healing in an *in Vitro* Model

Qing Zhang,[†,‡] Hua Dong,[†,‡] Yuli Li,[†,‡] Ye Zhu,[§] Lei Zeng,[†,‡] Huichang Gao,[†,‡] Bo Yuan,[†,‡] Xiaofeng Chen,[*,†,‡] and Chuanbin Mao[*,§,∥]

[†]Department of Biomedical Engineering, South China University of Technology, Guangzhou, Guangdong 510641, China

[‡]School of Materials Science and Engineering, South China University of Technology, Guangzhou, Guangdong 510641, China

[§]Department of Chemistry & Biochemistry, Stephenson Life Sciences Research Center, University of Oklahoma, Norman, Oklahoma 73019, United States

[∥]School of Materials Science and Engineering, Zhejiang University, Hangzhou 310027, China

ABSTRACT: Surface topography can affect cell adhesion, morphology, polarity, cytoskeleton organization, and osteogenesis. However, little is known about the effect of topography on the fracture healing in repairing nonunion and large bone defects. Microgrooved topography on the surface of bone implants may promote cell migration into the fracture gap to accelerate fracture healing. To prove this hypothesis, we used an *in vitro* fracture (wound) healing assay on the microgrooved polycaprolactone substrates to study the effect of microgroove widths and depths on the osteoblast-like cell (MG-63) migration and the subsequent healing. We found that the microgrooved substrates promoted MG-63 cells to migrate collectively into the wound gap, which serves as a fracture model, along the grooves and ridges as compared with the flat substrates. Moreover, the groove widths did not show obvious influence on the wound healing whereas the smaller groove depths tended to favor the collective cell migration and thus subsequent healing. The microgrooved substrates accelerated the wound healing by facilitating the collective cell migration into the wound gaps but not by promoting the cell proliferation. Furthermore, microgrooves were also found to promote the migration of human mesenchymal stem cells (hMSCs) to heal the fracture model. Though osteogenic differentiation of hMSCs was not improved on the microgrooved substrate, collagen I and minerals deposited by hMSCs were organized in a way similar to those in the extracellular matrix of natural bone. These findings suggest the necessity in using microgrooved implants in enhancing fracture healing in bone repair.

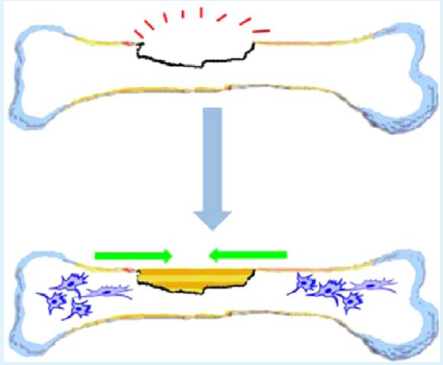

KEYWORDS: *collective cell migration, fracture healing, microgrooved topography, bone, implants*

1. INTRODUCTION

To satisfy the request of the development of regenerative medicine, the interaction between cells and their environment has been widely studied.[1−4] In bone tissue engineering, promoting nonunion fracture healing by implanting scaffolds is still a daunting challenge.[5−8] To tackle such challenge, it is very important to study the interaction between bone cells and the scaffolds.[9] It is now known that soluble factors,[10−12] topography,[13−16] stiffness[17] and composition of substrates,[18] and cell−cell contact[19,20] are cues that can affect the cell adhesion, proliferation, morphology, and differentiation. Among these cues, topography can avoid the side effect of soluble factors[21] and play a major role in extracellular matrix (ECM).[22] In the past 2 decades, many researchers have proved that topography can induce osteoblastic differentiation of mesenchymal stem cells (MSCs)[21,23] or affect osteoblast adhesion and morphology.[24,25]

Nonunion and large bone defects cause therapeutic challenges for surgeons.[26] To repair such defects, the biomaterials to be implanted should not only bear osteogenesis capacity but also favor the migration of cells into the fracture and the subsequent fracture healing. Fracture healing is a type of special wound healing,[27,28] and bony bridging of the peripheral callus across the fracture gap is a sign for successful fracture healing.[29] In addition, the long bone Haversian system and periosteum[30] are composed of oriented collagen fibers. These facts inspire us to hypothesize that oriented structures, such as parallel microgrooves on the bone-repairing material surface, could facilitate and guide the cells to grow along the microgrooves, which could in turn enhance the rate of fracture healing. So far, there has been no study on the effect of microgrooved substrates on collective cell migration along the microgrooves and the fracture healing.

Here, MG-63, a typical kind of human osteoblast-like cell,[31,32] was used as a model cell to investigate our hypothesis. Polycaprolactone (PCL) was chosen as a substrate material, as

Received: August 27, 2015
Accepted: October 6, 2015
Published: October 12, 2015

DOI: 10.1021/acsami.5b07976
ACS Appl. Mater. Interfaces 2015, 7, 23336−23345

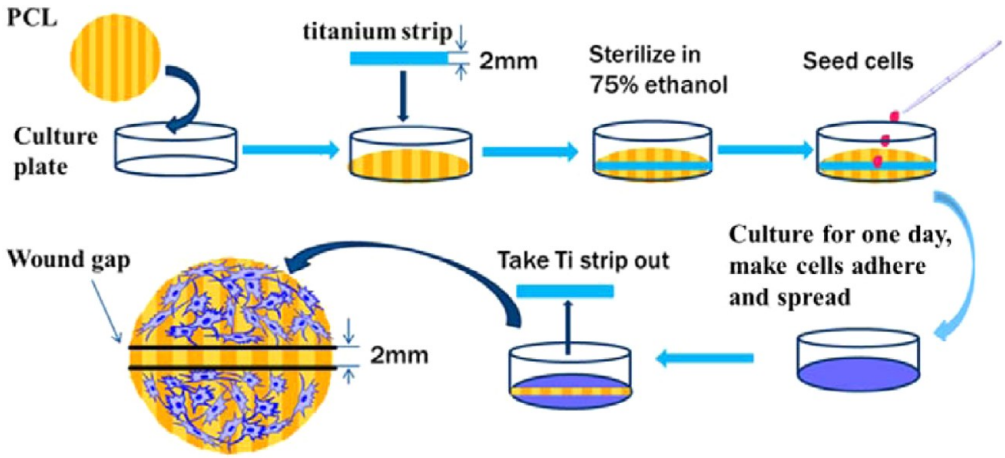

Figure 1. Operational flowchart of *in vitro* wound gap assay that is used to evaluate the use of microgrooved substrate for promoting fracture healing. Sterilized PCL substrates were first placed into a cell culture plate with a 2 mm wide titanium strip in the middle (titanium strip was perpendicular to the groove). Cells were seeded onto the PCL surface. After 24 h, the titanium strip was removed to generate a consistent 2 mm wound gap (a fracture model). MG-63 cells were allowed to grow into the wound gap for 2, 4, 6, and 8 days. hMSCs were allowed to grow into the wound gap for 1 and 2 days.

it is approved by the U.S. Food and Drug Administration (FDA) for its biocompatibility and clinical applications. The microgrooved PCL substrates were prepared by a combination of photolithography and melt-casting methods. A standard *in vitro* wound healing assay[33] on the microgrooved substrates (Figure 1) was then employed to test the response of MG-63 cells to PCL substrates with various microgrooved widths and depths. In addition, hMSCs were used to test the wound healing and the osteogenic differentiation of hMSCs on the microgrooved substrates was characterized. To the best of our knowledge, this is the first time that the influence of micropatterned material on MG-63 and hMSCs wound healing rate is reported.

2. EXPERIMENTAL SECTION

2.1. Substrate Fabrication. Microgrooved PCL substrates were fabricated by a combination of standard soft photolithography and melt-casting techniques. Silicon wafers (from Set Crystal Silicon Management Department, ⟨111⟩) were washed with sulfuric acid and hydrogen peroxide mixture (ratio of 7:3, v/v), followed by a sequential rinsing with isopropyl alcohol, acetone, and deionized water. AR grade sulfuric acid, hydrogen peroxide, isopropyl alcohol, and acetone were purchased Guangzhou Chemical Reagent Factory. Deionized water was produced by a water purification system (Millipore S.A.S.). After drying with nitrogen (from Guangzhou Sheng Ying Gas Limited Company, China), a negative photoresist (Futurrex, NR21-20000P, USA) was spin-coated on the cleaned silicon wafers to form a uniform film with the thickness of 25, 50, and 100 μm, respectively. Master molds were produced by transferring photomask (Shenzhen Microcad Photomask LTD, China) patterns to the photoresist according to the manufacture's protocol. Polydimethylsiloxane (PDMS, Sylgard 184, Dow Corning, USA) templates with defined topographies were then created by pouring elastomer and curing agent (ratio of 10:1, w/w) over the photoresist master and heating on a hot plate (Shanghai Chamet Function ceramics Technology Limited Company, ModelKw-4AH, China) at 60 °C for 4 h. PCL (MW = 60 000, Dai Gang Biology, China). Substrates were produced by melting PCL particles on PDMS templates. Prior to use, all PCL samples were sterilized in 75% AR grade ethanol (Guangzhou Chemical Reagent Factory, China) for 24 h and rinsed by a phosphate buffer solution (PBS).

Table 1. Primers Used for Real-Time PCR Analysis

gene	primer 5′-3′
GAPDH	F: 5′-AGAAAAACCTGCCAAATATGATGAC-3′
	R: 5′-TGGGTGTCGCTGTTGAAGTC-3′
ALP (alkaline phosphatase)	F: 5′-AGCACTCCCACTTCATCTGGAA-3′
	R: 5′-GAGACCCAATAGGTAGTCCACATTG-3′
OCN (osteocalcin)	F: 5′-CAGCGAGGTAGTGAAGAGA-3′
	R: 5′-GACTGGTGTAGCCGAAAG-3′
Col I (collagen I)	F: 5′-CAGCCGCTTCACCTACAGC-3′
	R: 5′-TTTTGTATTCAATCACTGTCTTGCC-3′
OPN (osteopontin)	F: 5′-GCGAGGAGTTGAATGGTG-3′
	R: 5′-CTTGTGGCTGTGGGTTTC-3′

2.2. Cell Culture Preparation. MG-63 cells were cultured in a low glucose Dulbecco's modified Eagle medium (DMEM, Gibco, Life Technologies, USA) containing 10% fetal bovine serum (FBS, Gibco, Life Technologies, USA) at 37 °C in a humidified incubator (HERAcell 240i, Thermo, USA) with 5% CO_2:95% air atmosphere.

hMSCs were purchased from Cyagen Biosciences. They were cultured in DMEM with 10% FBS and 1% penicillin/streptomycin antibiotics (all from Cyagen Biosciences) at 37 °C and with 5% CO_2 in a 75 cm^2 culure flask (Corning, USA). hMSCs were used in the experiment at passage seven.

2.3. *In Vitro* Wound Healing Assay. Wound healing assay was used to evaluate the *in vitro* rate of cells wound gap healing on different microgrooved substrates (as shown in Figure 1). Sterilized PCL substrates were first placed into a 24-well cell culture plate (Corning, USA) with a 2 mm wide titanium strip in the middle (titanium strip was perpendicular to grooves). Cells were then suspended in 1 mL culture media (4×10^4 cells per mL) and seeded onto each PCL surface. After 24 h, the titanium strip was removed to generate a consistent 2 mm wound gap. MG-63 cells were allowed to grow into the wound gap for 2, 4, 6, and 8 days. hMSCs were allowed to grow into the wound gap for 1 and 2 days. After being immersed in a 4% formaldehyde (Guangzhou Chemical Reagent Company, AR grade, China) solution for 30 min, cells were permeated with 0.1% Triton X-100 (UNI-Chem, Serbia). They were then incubated with phalloidin-FITC (AAT Bioquest, USA) and DAPI (Beyotime, China) sequentially. Images of the wound gap were taken by an inverted fluorescence microscope (Eclipsc Ti-U, Nikon, Japan) and a laser scanning confocal microscope (LSCM, Leica SP5, Germany) to analyze the gap distance. At least three representative points along the wound of each sample were used to evaluate the gap distance in four separate samples. Three independent experiments were performed.

DOI: 10.1021/acsami.5b07976
ACS Appl. Mater. Interfaces 2015, 7, 23336−23345

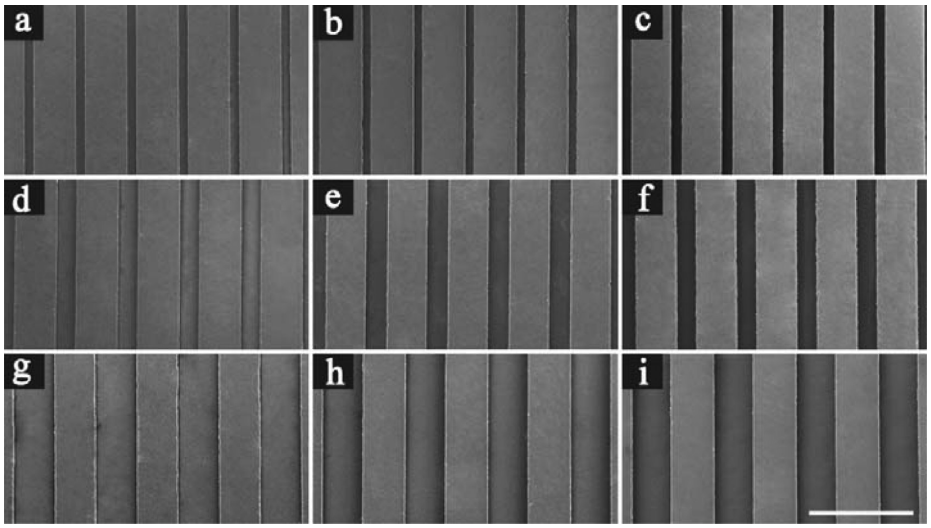

Figure 2. Top to bottom: SEM images of microgrooved PCL substrates with the groove depth in the range of 25, 50, 100 μm and the groove width in the range of 50, 100, 200 μm: (a) D25W50; (b) D50W50; (c) D100W50; (d) D25W100; (e) D50W100; (f) D100W100; (g) D25W200; (h) D50W200; (i) D100W200. Scale bar = 500 μm.

2.4. Osteogenic Differentiation of hMSCs. To assess the osteogenic differentiation of hMSCs on the microgrooved substrates, hMSCs were seeded on the flat and D25W200 substrates at a density of 4×10^4 cells/well with a 2 mm wide titanium strip in the middle. Then the strip was removed after 24 h as described above. hMSCs continued to be cultured for 2 days in the complete culture medium. The cells were then cultured in osteogenesis inducing media with 10 mM β-glycerophosphate, 50 μg ascorbic acid, and 10 nM dexamethasone. The media were refreshed every 3 days.

2.5. Cell Proliferation. Proliferation of MG-63 cells on the PCL substrates was determined by a Cell Counting Kit-8 assay (CCK-8, Dojindo Laboratories, Kumamoto, Japan). Suspended cells were seeded at a density of 4×10^4 mL^{-1} on the PCL substrates, each of which was placed in a well of a 24-well cell culture plate (Corning, USA). Samples were harvested on the 1st, 3rd, 5th, and 7th days (four samples for each group for each time point). Each well was incubated in a 200 μL DMEM medium containing 20 μL of CCK-8 reagent under normal culture conditions for 1 h. 100 μL of the medium was then extracted and added into a new 96-well plate (Corning, USA) and the absorbance was measured at a wavelength of 450 nm using Thermo Scientific Microplate Reader (Thermo3001, USA).

2.6. Characterization of Cell Morphology. Morphology of cells cultured on PCL substrates was analyzed by laser scanning confocal microscopy (LSCM, Leica SP5, Germany). F-actin and cell nucleus were stained by phalloidin-FITC and DAPI, respectively. The samples were prepared as described in section 2.3 *in vitro* wound healing assay.

2.7. Alkaline Phosphatase Activity Analysis. The intracellular alkaline phosphatase (ALP) activity was evaluated quanlitatively and quantitatively using commercially available kits. In the qualitative assay, after osteogenic induction for 7 and 14 days, hMSCs on the substrates were washed three times with phosphate buffered saline (PBS), fixed with 10% formaldehyde, then stained with BCI/NBT ALP Color Development Kit (Beyotime). In the quantitative assay, hMSCs were washed three times with PBS, then lysed in 300 μL of lysate for 1 h on ice. Cell lysis solution contained 10 mM Tris−HCl (pH = 7.4), 0.5 mM $MgCl_2$, and 0.1% triton X-100. The ALP activity in the lysate was evaluated colorimetrically with the Alkaline Phosphatase Assay Kit (P0321, Beyotime, China), which was based on the conversion of colorless *p*-nitrophenyl phosphate (pNPP) to colored *p*-nitrophenol after coincubation for 15 min at 37 °C. The results were normalized to the total intracellular protein content determined by the bicinchoninic acid (BCA) Protein Assay Kit (23225, Thermo scientific, USA). The results were expressed in nanomoles of produced *p*-nitrophenol per min per milligram of protein.

2.8. Real-Time Quantitative PCR Analysis. hMSCs cultured on the flat and D25W200 substrates were collected on days 3 and 21. Total RNA was extracted by using HiPure Total RNA Micro Kit (R-1114-03, Magen). Afterward, cDNA was synthesized from 500 ng of RNA using Reverse Transcription Reagents Kit (RR047A, Takara) according to the manufacturer's instructions. The real-time PCR was performed in QuantStudio 6 Flex (Life technologies) using the Maxima SYBR Creen/ROX qPCR (K0222, Thermo Scientific). The C_T value for each gene of interest was normalized to the corresponding C_T value of housekeeping gene GAPDH. The relative fold change of each gene was calculated with the $\Delta\Delta C_T$ method against control group. The primer sequences of selected gene for real-time PCR are listed in Table 1.

2.9. Immunofluorescence of Collagen I. After 21 days of culture, hMSCs were fixed in 4% formaldehye for 20 min at 4 °C and then incubated in 10% fetal bovin serum (FBS) for 20 min to block nonspecific protein−protein interactions. The samples were incubated with the Anticollagen I antibody (ab90395, Abcam, USA, 1/2000) overnight at 4 °C. The secondary antibody, Goat antimouse IgG, Cy3 conjugated (CW0145, CWBIO, China), was used at 1/200 dilution for 1 h.

2.10. Extracellular Matrix Mineralization Assay. The degree of extracellular matrix mineralization was determined by Alizarin Red S (A100195, Alfa Aesar, USA). Briefly, after osteogenic induction for 21 days, cells were fixed with 10% formaldehyde for 30 min, washed three times by ultrapure water, then stained with 0.5% Alizarin Red S (pH 4.2) for 5 min at room temperature. Afterward, the unbound stain was totally removed by rinsing with ultrapure water. Quantitative analysis of Alizarin Red S staining was performed by eluting the bound stain with 500 μL of 10% cetylpyridiium chloride in 10 mM Na_2HPO_4 (pH 7.0) for 1 h. The absorbance of the resulting solution was measured using the microplate reader (Thermo3001, Thermo, USA) at a wavelength of 562 nm.

2.11. Statistical Analysis. An unpaired student's *t* test was used to evaluate the significance among experiment groups. Results were further divided into "statistically significant" (*, $0.01 < p < 0.05$) and "very significant" (**, $P < 0.01$). One-way analysis of variance was used to evaluate the corresponding effect of the groove width and depth on the wound healing.

3. RESULTS

3.1. Morphology of Topographically-Patterned PCL Substrates. Microgrooved PCL substrates were prepared by combining soft-photolithography and melt-casting. To achieve

DOI: 10.1021/acsami.5b07976
ACS Appl. Mater. Interfaces 2015, 7, 23336−23345

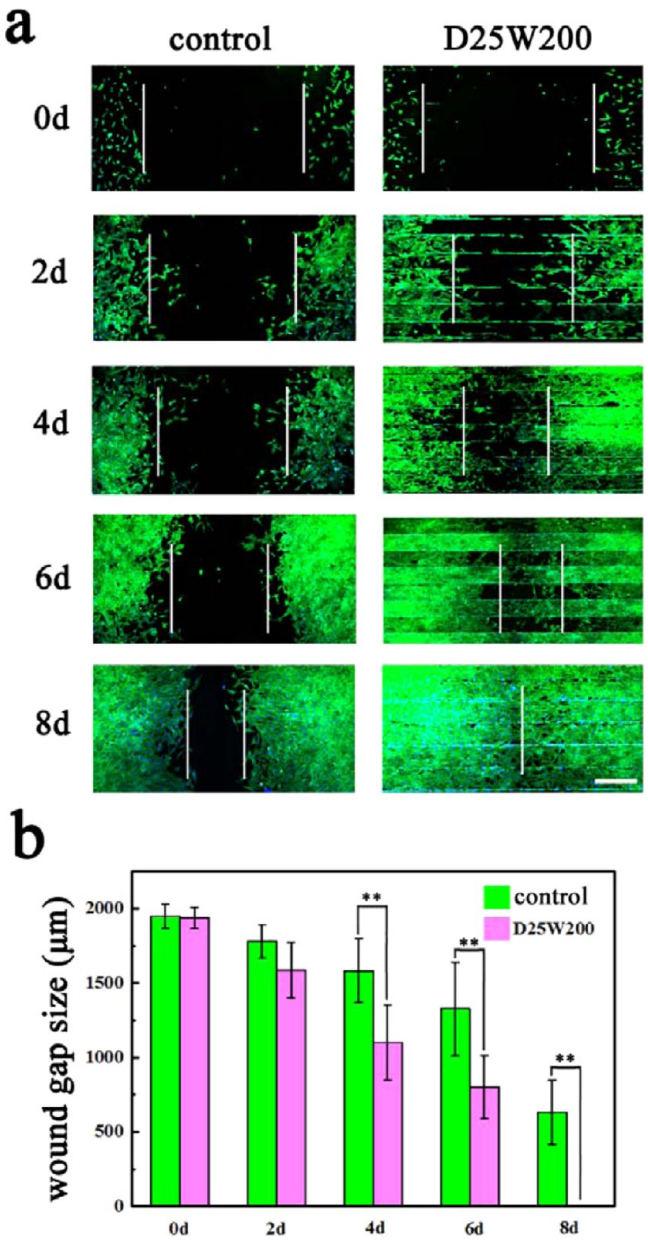

Figure 3. *In vitro* wound healing assay on the flat and D25W200 substrates. MG-63 cells were seeded at a density of 4×10^4 on each substrate with an insert titanium trip in the middle. After 24 h, the inset was removed to generate a 2 mm "wound gap". Cells were allowed to migrate into the wound gap and were visualized using DAPI and FITC-phalloidin staining: (a) fluorescence images of wound gap on the 0th, 2nd, 4th, and 6th day after the removal of titanium trips and (b) quantification of the "wound gap" distance between the front lines of migrating MG-63 cells. ** Statistically significant, $p < 0.01$. Scale bar = 500 μm.

a high fabrication yield, the width of ridges between microgrooves was set at 200 μm for all PCL samples, whereas the width and depth of microgrooves changed (25, 50, 100, and 200 μm). Figure 2 shows the SEM images of microgrooved PCL substrates. The surfaces of the samples are clean and free of impurity particles. The microgroove features such as the shape and size are in good accordance with the design. PCL samples are labeled in the following section by a numbering format such as D25W50 (depth, 25 μm; groove width, 50 μm) and D50W100 (depth, 50 μm; groove width, 100 μm). The flat PCL samples fabricated by the same method were used as a control group.

3.2. Wound Gap Healing Affected by Microgrooved PCL Substrates. *In vitro* wound healing assays (Figure 1) were performed to investigate the rate of wound gap healing affected by microgrooved substrates. For MG-63 wound gap healing, fluorescence images were taken on the 0th, 2nd, 4th, 6th, and 8th day after the titanium strip was removed. It should be noted that cells had already been cultured for 1 day before the titanium strip was removed. The gap of each wound at every time point was measured and the wound advancing rate was quantified. Compared with control, wound gap healing was increased on D25W200 substrate (Figure 3). Immediately after the removal of the titanium strip, the widths of wound gaps are quite close on the control and D25W200 substrates (~2000 μm). On the 2nd day, the wound advances ~90 μm and ~150 μm on the control and D25W200 substrates, respectively. This trend is further enhanced with the prolonged culture time. After 6 days of culture time, the average wound gap healing rate on the D25W200 is ~210 μm/day, which is more than twice as much as that on the control substrate (~100 μm/day, consistent with other researchers' results[34]). On the 8th day, the wound gap on D25W200 substrates healed, but the distance of wound gap on control was about 650 μm.

Furthermore, the individual effect of groove width and depth on MG-63 wound gap healing was investigated. MG-63 wound gap healing rates on all of the microgrooved substrates are dramatically increased as compared to the flat substrates. Interestingly, substrates with different groove depths, but the same widths (Figure 4) exhibit a significant difference between each other. However, substrates with various groove widths but having the same depth (Figure 4) show negligible differences. This implies that the groove depth plays a more important role in wound healing. Moreover, substrates with a groove depth of 25 μm show the best promotional effects.

The effect of microgrooves on the healing of the wound gaps by hMSCs was also investigated. Compared with control, wound gap healing was greatly increased on D25W200 substrate (Figure 5). Besides, the rate of hMSCs wound gap healing was much faster than MG-63 wound gap healing. On the 2nd day, the hMSCs wound gap on D25W200 substrates was healed, but the distance of wound gap on control was about 1000 μm.

3.3. MG-63 Cell Proliferation. CCK-8 assays were conducted to measure the cell proliferation behavior. Cell density was then calculated by dividing the total cell number by the apparent covered surface area. As depicted in Figure 6, a rapid increase in cell density between the time points proves that the cell proliferation behavior on these samples is normal. There are no significant differences between cell proliferation behavior on the 1st and the 3rd days. However, on the 5th and the 7th days, proliferation behavior is affected to a large extent by the groove depth; the higher cell numbers are associated with the deeper grooves.

3.4. MG-63 Cell Morphology on Microgrooved Substrates. The morphology of MG-63 cells was analyzed by LSCM. MG-63 cells spread in a normal manner and exhibited a random arrangement on the flat substrates on the 1st and the 3rd day. In contrast, cells were oriented in a direction parallel to the groove once they were near or on the edge of the ridge on the 1st day (as indicated by the red arrows in Figure 7b) and the 3rd day. Cell F-actin was also assembled in an orientation that reflected the elongated cell shape. Nuclei

DOI: 10.1021/acsami.5b07976
ACS Appl. Mater. Interfaces 2015, 7, 23336−23345

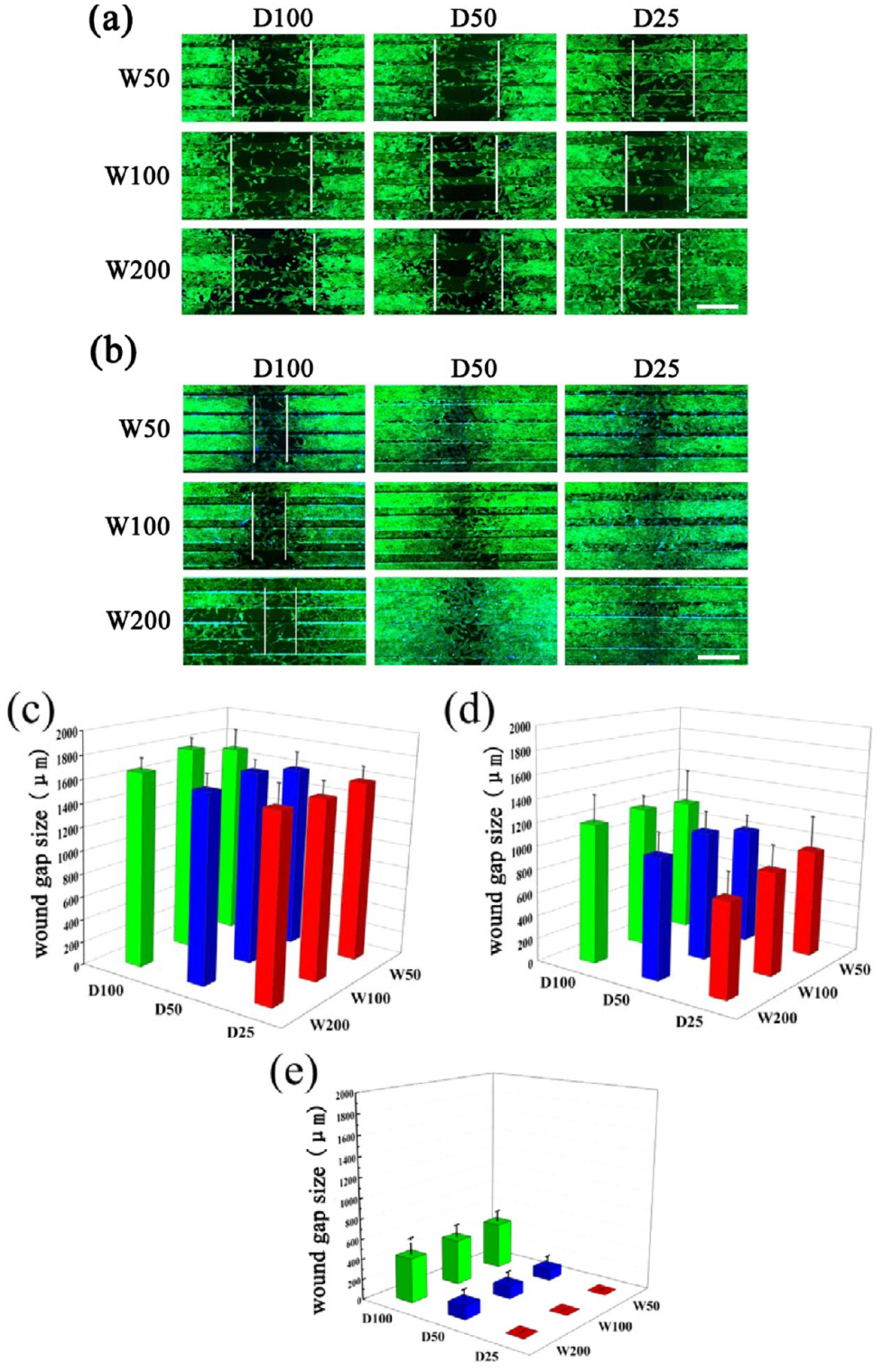

Figure 4. Results of *in vitro* wound healing assay on all types of substrates. One-way analysis of variance was used to investigate the individual effect of groove width and depth on wound healing: (a) and (b) are fluorescence images of wound gap on the different substrates on the 6th day (a) and 8th day (b) after the removal of titanium strips. Data on the 0th, 2nd, and 4th day are not shown. Panels c, d, and e are quantification of the "wound gap" distance between the front lines of migrating MG-63 cells on the different substrates on the 2nd day (c), 6th day (d), and 8th day (e) after the removal of titanium trips. Data on the 0th and 4th day are not shown. Scale bar = 500 μm.

of the oriented cells also exhibited a preferential orientation[35,36] on the 1st and the 3rd day (Figure 7b,d). The cells on the bottom and top platform of microgrooved substrates were of particular interest. They spread in a normal manner and exhibited a random arrangement on the 1st day similar to the cells on the flat substrates (Figure 7b). However, on the 3rd day, these collective cells (with the cell proliferation) were oriented in the direction parallel to the groove and ridge on the microgrooved substrates, while their nuclei did not exhibit a preferential orientation (Figure 7d).

DOI: 10.1021/acsami.5b07976
ACS Appl. Mater. Interfaces 2015, 7, 23336−23345

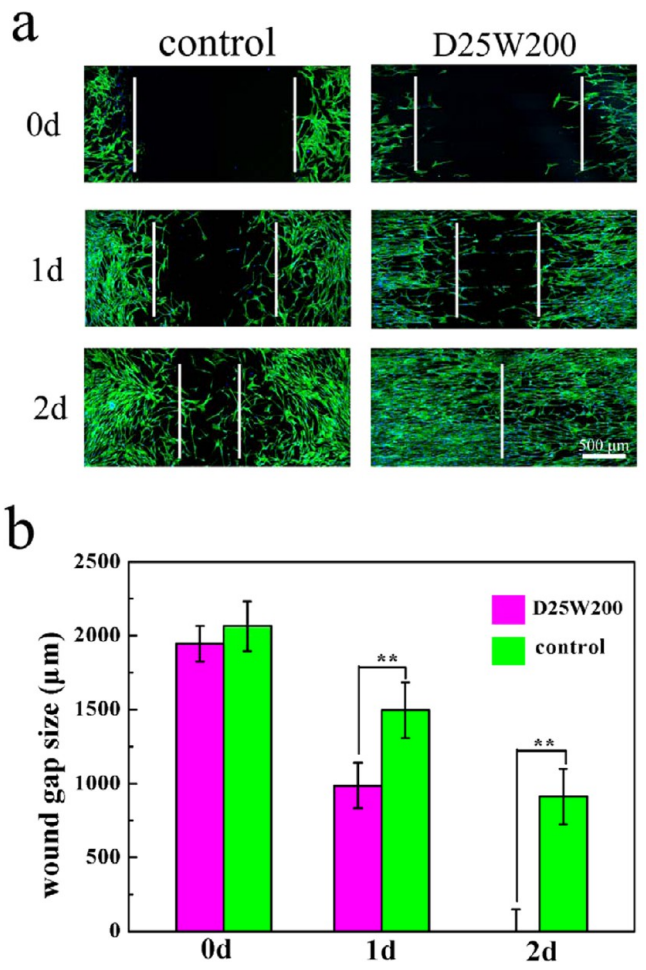

Figure 5. *In vitro* wound healing assay on the flat and D25W200 substrates. hMSCs were seeded at a density of 4 × 10^4 on each substrate with an insert titanium trip in the middle. After 24 h, the inset was removed to generate a 2 mm "wound gap". Cells were allowed to migrate into the wound gap and were visualized using DAPI and FITC-phalloidin staining: (a) fluorescence images of wound gap on the 0th, 1st, and 2nd day after the removal of titanium trips and (b) quantification of the "wound gap" distance between the front lines of migrating hMSCs. ** Statistically significant, $p < 0.01$. Scale bar = 500 μm.

3.5. Osteogenic Differentiation of hMSCs. To investigate the role of microgrooves in osteogenic differentiation, expression of osteogenic markers and mineralization of hMSCs on the flat and D25W200 substrates were tested. ALP, a kind of glycoprotein on the cell membrane of osteoblasts,[37] is widely used as a marker of the osteogenic phenotypes. The ALP activity of hMSCs was measured using cell samples collected on days 7 and 14. As shown in Figure 8a and 8b, the ALP activity level of hMSCs was slightly increased for the D25W200 substrates compared with control on day 7, but no statistical difference was found on day 14. The result of extracellular marix mineralization is similar to that of ALP activity. No significant difference can be observed between D25W200 and control group (data not shown). In addition, the expression levels of the osteogenic markers (collagen I, OPN, OCN and ALP) on the D25W200 substrates were not increased in comparison to the control group on days 3 and 21 (Figure 8c). However, immunofluorescence staining of collagen I and alizarin red S staining (Figure 9) indicate that collagen I and

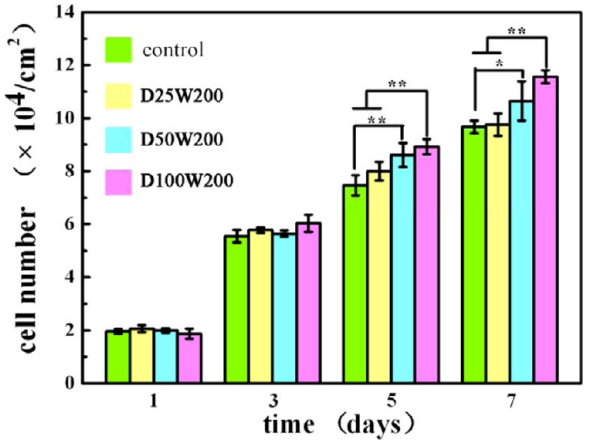

Figure 6. MG-63 cell proliferation measured by CCK-8 assays on the flat, D100W200, D50W200 and D25W200 substrates. Cell density was calculated by dividing the total cell number by the apparent covered surface area. Statistically significant, ** $p < 0.01$, * $0.01 < p < 0.05$.

mineral CaP were aligned in a way similar to the natural organization in bone.

4. DISCUSSION

PCL is a type of excellent bone-repairing material.[38,39] A combination of standard soft photolithography and melt-casting techniques was cost-effective (as opposed to thermo-compression formation or laser instrument) and easy to operate in preparing the topography on thermoplastic polymer surfaces. Residual solvent contamination was also avoided by using this technology. Repeated tests proved that a combination of standard soft photolithography and melt-casting was an accurate method to produce a large number of microstructures as designed on PCL substrates.

Fracture repair is a complex and multifactorial process.[29,40] It is thought to be based on the interaction between three elements: cell biology of bone regeneration, revascularization of devitalized bone, and soft tissue adjacent to the fracture.[41] Cell biology involves a number of cellular events such as adhesion, migration,[42] proliferation and differentiation,[34,43] and apoptosis.[42] The coordination is ensured by cytokines, growth factors, nutrients, pH, oxygen tension,[44] surface properties,[45] and physicochemical properties of biomaterials.[46] Topography, as a kind of surface property of biomaterials and ECM, can influence cell adhesion, morphology, migration, proliferation, and differentiation.[23,47−49] In this study, microgrooves, which are similar to Haversian system and surface morphology of periosteum, distinctly promote MG-63 wound gap healing. Groove depth is more effective than the groove width on the healing rate. Possible changes in cell proliferation and collective cell migration were investigated to elucidate the mechanism.

Cell proliferation did not show significant statistical differences between D25W200 and the control substrates on the 1st, 3rd, 5th, and 7th day (Figure 6). Cell proliferation rate on D50W200 and D100W200 was faster than that on D25W200 and control substrates. Nevertheless, the relationship between cell proliferation and groove depth is not in agreement with the findings that the wound healing rate increases as the groove depth decreases. These results indicate that acceleration of wound gap healing on microgrooved substrates is not a result of MG-63 cell proliferation behavior. In addition, LSCM images demonstrate that collective MG-63 cell morphology on the

DOI: 10.1021/acsami.5b07976
ACS Appl. Mater. Interfaces 2015, 7, 23336−23345

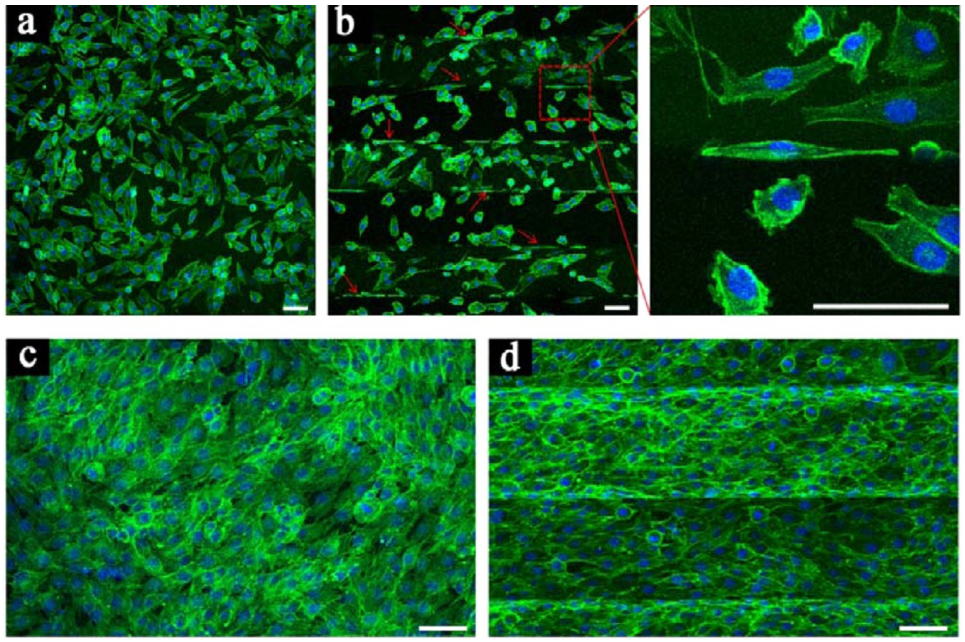

Figure 7. Characterization of MG-63 cell adhesion and spreading on the flat and topographically patterned substrates. Laser scanning confocal microscopy images were taken after MG-63 cells were cultured (a) on a flat substrate for 1 day, (b) on D25W200 substrate for 1 day, (c) on a flat substrate for 3 days, and (d) on D25W200 substrate for 3 days. Red arrows indicate aligned cells. Scale bar = 100 μm.

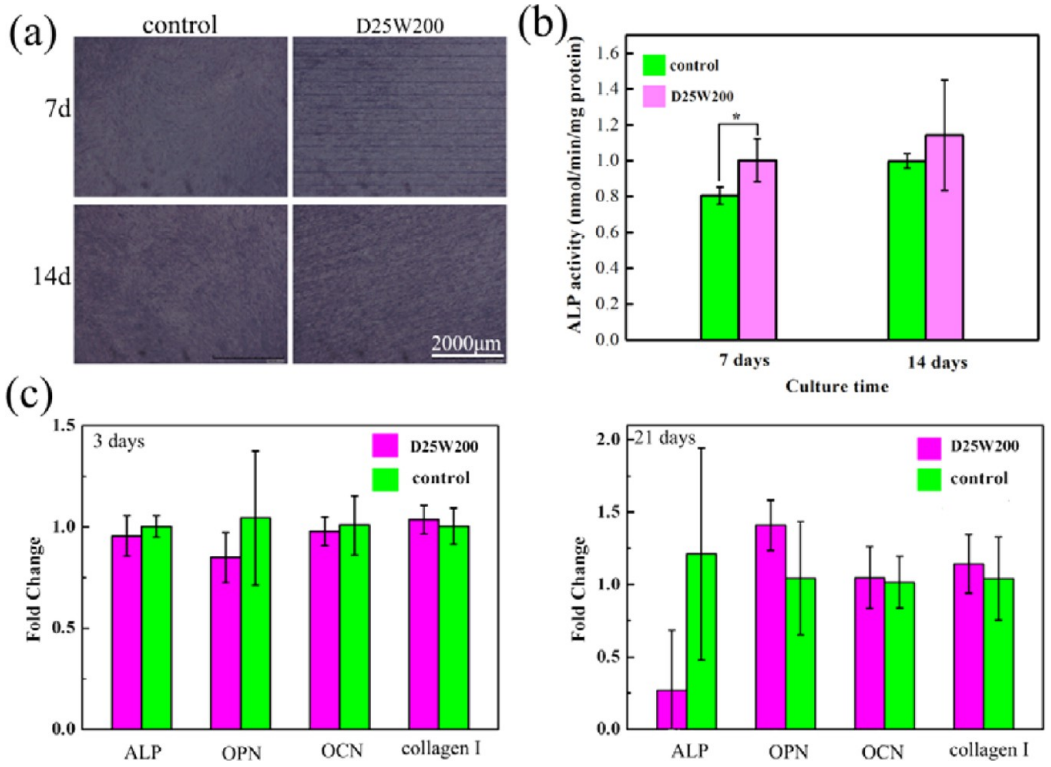

Figure 8. Osteogenic differentiation of hMSCs on flat and D25W200 substrates. (a) ALP staining and (b) ALP activity of hMSCs cultured on the flat and D25W200 substrates after osteogenic induction for 7 and 14 days. (c) qPCR analysis of osteogenic marker genes of hMSCs cultured on the flat and D25W200 substrates after osteogenic induction for 3 and 21 days.

microgrooved substrates was quite different from that on the flat substrates (Figure 7). Collectively, MG-63 cells were oriented along the groove and ridge on the microgrooved substrates on the 3rd day, and spread in a normal manner on the flat substrates. It suggests that the cells near or on the edge of ridge first sense the topography and are directed along the direction parallel to the groove and ridge (Figure 7b). As cellular proliferation progresses, the cells experiencing contact guidance by the groove could meet the other cells in the middle of the groove and transfer the information to them.[50] Finally, a group of cells elongates along the microgroove[35,36] (Figure 7d). The collective MG-63 cell migration is also directed by the

DOI: 10.1021/acsami.5b07976
ACS Appl. Mater. Interfaces 2015, 7, 23336−23345

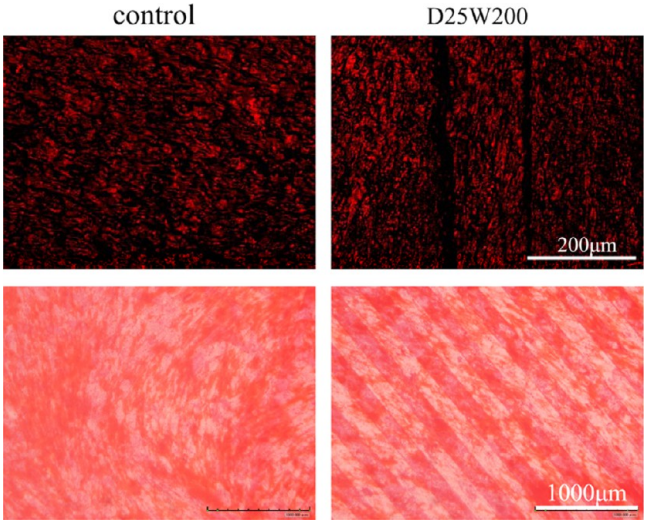

Figure 9. Upper is immunofluorescence staining of collagen I of hMSCs cultured on the flat and D25W200 substrates after osteogenic induction for 21 days. The lower is alizarin red S staining of hMSCs cultured on the flat and D25W200 substrates after osteogenic induction for 21 days.

microgrooved topography. This result is consistent with previous studies. Specifically, the myofibroblasts elongate along the anisotropic collagen-containing nanofibers and consequently their migration was promoted.[51] Parallel microgrooves increases endothelial cell migration rates.[52,53] Corneal epithelium cells were directed to migrate along the parallel grooves[54] (groove and ridge width of 1, 2, 5, and 10 μm, groove depth of 1 and 5 μm). These effects are different from the effect of nanoparticles on cellular migration, which strengthened intracellular tension and retard cellular migration.[55] However, it is likely that adding nanoparticles to the microgrooved substrates would tune the migration behaviors of the cells to some extent.

MG-63 proliferation was not affected by the topographic patterns within the 3 days, but became faster with an increase in groove depth on the 5th and 7th culturing day (cultured on D25W200, D50W200, and D100W200 substrates). Because MG-63 cells do not form multicellular aggregates within the microgrooves, the proliferation is undoubtedly modulated by available substrate area. All substrates have enough surface area for MG-63 cell proliferation for 3 culture days. After this period, deeper groove substrates possess larger surface area for cell adhesion, which is beneficial for the cell proliferation. Within the initial 3 days, cell density on D25W200 was larger than that on the deeper groove substrates. Therefore, cell−cell contact was more frequent and more information was transmitted, resulting in the elongation of more cells along the groove and ridge. In the initial culture days, collective cell migration on D25W200 is faster than that on the deeper substrates (Figure 4). During the following culture days, cells on D25W200 become in closer contact as the cells proliferate further, which in turn promote the collective cell migration. More space for cell growth is available in the D100W200 due to its larger surface area with deeper side walls. Cell proliferation on the deeper substrates is faster on the 5th and 7th culture day. Although there is enough surface area, cells do not come in close contact as opposed to what happens on the D25W200 substrates. Finally, substrates with a groove depth of 25 μm show the best promotional effects (Figure 4e).

There is no difference between D25W200 substrates and control group for the osteogenesis ability of hMSCs. PCL as a traditional biomaterial is biocompatible and has a high differentiation potential.[56,57] Therefore, comparing flat control with the grooved group did not show many significant differences in terms of differentiation potential. In addition, nanotopography can affect cell differentiation;[37,58] however, microtopography usually influences collective cell behavior.[59] In this study, mirogrooved topography can promote collective cell migration but do not improve the osteogenesis ability of hMSCs as reported by others.[60] Microgrooved topography influenced hMSCs morphology and collective cell behavior. Microgrooves not only accelerate the hMSCs wound gap healing but also influence the organization of collagen I and minerals secreted by the stem cells. Cells were found to be aligned along the grooves. Consequently, collagen I and minerals deposited by the cells were in a aligned pattern.[37] Such alignment was similar to the organization of the same components in natural bone. It is known that hydroxyapatite crystals can be formed in the space between highly organized collagen I fibrils.[61]

5. CONCLUSION

This study was performed to evaluate whether the wound healing process could be directed and facilitated by an underlying polymer having a surface geometry of parallel grooves. Results confirmed that microgrooved substrates could promote MG-63 wound gap healing along the groove and ridge as compared with the flat substrates. This promotional effect was caused by microgroove-enhanced collective MG-63 cell migration but not by accelerating cell proliferation. The influence of different groove widths on wound healing is not obvious. However, the depth shows a significant influence; the more shallow groove promotes the collective cell migration. Substrates with a groove depth of 25 μm show the best promotional effects (more than 2 times as much as that on the control substrate). Collective cell migration significantly contributes to the difference in wound healing process. Besides, collagen I and minerals deposited by hMSCs in the osteogenesis inducing media on the D5W200 substrates were organized in a similar pattern to the extracellular matrix of natural bone. These findings suggest that the microgrooved surface can be potentially used for promoting the fracture healing process.

AUTHOR INFORMATION

Corresponding Authors

*X. Chen. E-mail: chenxf@scut.edu.cn.
*C. B. Mao. E-mail: cbmao@ou.edu.

Notes

The authors declare no competing financial interest.

ACKNOWLEDGMENTS

This work was financially supported by the National Basic Research Program of China (Grant No. 2011CB606204 and 2012CB619100), the National Natural Science Foundation of China (Grant No. 51172073 and 51202069), and the Specialized Research Fund for the Doctoral Program of Higher Education of China (Grant No. 20110172120002). Y.Z. and C.B.M. thank the financial support from National Institutes of Health (EB015190), National Science Foundation (CMMI-1234957 and CBET-1512664), Department of Defense office

DOI: 10.1021/acsami.5b07976
ACS Appl. Mater. Interfaces 2015, 7, 23336−23345

of the Congressionally Directed Medical Research Programs (W81XWH-15-1-0180), Oklahoma Center for Adult Stem Cell Research (434003), and Oklahoma Center for the Advancement of Science and Technology (HR14-160).

REFERENCES

(1) Ke, H.; Wang, H.; Wong, W. K.; Mak, N. K.; Kwong, D. W.; Wong, K. L.; Tam, H. L. Responsive and Mitochondria-Specific Ruthenium(Ii) Complex for Dual in Vitro Applications: Two-Photon (near-Infrared) Induced Imaging and Regioselective Cell Killing. *Chem. Commun. (Cambridge, U. K.)* **2010**, *46*, 6678−6680.

(2) Chen, C. S.; Jiang, X. Y.; Whitesides, G. M. Microengineering the Environment of Mammalian Cells in Culture. *MRS Bull.* **2005**, *30*, 194−201.

(3) Yao, X.; Peng, R.; Ding, J. Cell-Material Interactions Revealed Via Material Techniques of Surface Patterning. *Adv. Mater.* **2013**, *25*, 5257−5286.

(4) Zhu, H.; Cao, B.; Zhen, Z.; Laxmi, A. A.; Li, D.; Liu, S.; Mao, C. Controlled Growth and Differentiation of Mscs on Grooved Films Assembled from Monodisperse Biological Nanofibers with Genetically Tunable Surface Chemistries. *Biomaterials* **2011**, *32*, 4744−4752.

(5) Thibault, R. A.; Mikos, A. G.; Kasper, F. K. Scaffold/Extracellular Matrix Hybrid Constructs for Bone-Tissue Engineering. *Adv. Healthcare Mater.* **2013**, *2*, 13−24.

(6) Surmenev, R. A.; Surmeneva, M. A.; Ivanova, A. A. Significance of Calcium Phosphate Coatings for the Enhancement of New Bone Osteogenesis–a Review. *Acta Biomater.* **2014**, *10*, 557−579.

(7) Reichert, J. C.; Hutmacher, D. W. Bone Tissue Engineering. *Tissue Eng.* **2011**, 431−456.

(8) Wang, J.; Yang, M.; Zhu, Y.; Wang, L.; Tomsia, A. P.; Mao, C. Phage Nanofibers Induce Vascularized Osteogenesis in 3d Printed Bone Scaffolds. *Adv. Mater.* **2014**, *26*, 4961−4966.

(9) Anselme, K.; Ponche, A.; Bigerelle, M. Relative Influence of Surface Topography and Surface Chemistry on Cell Response to Bone Implant Materials. Part 2: Biological Aspects. *Proc. Inst. Mech. Eng., Part H* **2010**, *224*, 1487−1507.

(10) Simonet, W. S.; Lacey, D. L.; Dunstan, C. R.; Kelley, M.; Chang, M. S.; Luthy, R.; Nguyen, H. Q.; Wooden, S.; Bennett, L.; Boone, T.; Shimamoto, G.; DeRose, M.; Elliott, R.; Colombero, A.; Tan, H. L.; Trail, G.; Sullivan, J.; Davy, E.; Bucay, N.; RenshawGegg, L.; Hughes, T. M.; Hill, D.; Pattison, W.; Campbell, P.; Sander, S.; Van, G.; Tarpley, J.; Derby, P.; Lee, R.; Boyle, W. J. Osteoprotegerin: A Novel Secreted Protein Involved in the Regulation of Bone Density. *Cell* **1997**, *89*, 309−319.

(11) Kong, Y. Y.; Yoshida, H.; Sarosi, I.; Tan, H. L.; Timms, E.; Capparelli, C.; Morony, S.; Oliveira-dos-Santos, A. J.; Van, G.; Itie, A.; Khoo, W.; Wakeham, A.; Dunstan, C. R.; Lacey, D. L.; Mak, T. W.; Boyle, W. J.; Penninger, J. M. Opgl Is a Key Regulator of Osteoclastogenesis, Lymphocyte Development and Lymph-Node Organogenesis. *Nature* **1999**, *397*, 315−323.

(12) Shinozaki, Y.; Toda, M.; Ohno, J.; Kawaguchi, M.; Kido, H.; Fukushima, T. Evaluation of Bone Formation Guided by DNA/Protamine Complex with Fgf-2 in an Adult Rat Calvarial Defect Model. *J. Biomed. Mater. Res., Part B* **2014**, *102*, 1669−1676.

(13) Dalby, M. J.; McCloy, D.; Robertson, M.; Agheli, H.; Sutherland, D.; Affrossman, S.; Oreffo, R. O. C. Osteoprogenitor Response to Semi-Ordered and Random Nanotopographies. *Biomaterials* **2006**, *27*, 2980−2987.

(14) McNamara, L. E.; Dalby, M. J.; Tsimbouri, M. P. The Use of Microarrays and Fluorescence in Situ Hybridization for the Study of Mechanotransduction from Topography. *Methods Cell Biol.* **2014**, *119*, 293−309.

(15) Wang, J.; Wang, L.; Li, X.; Mao, C. Virus Activated Artificial Ecm Induces the Osteoblastic Differentiation of Mesenchymal Stem Cells without Osteogenic Supplements. *Sci. Rep.* **2013**, *3*, 1242.

(16) Wang, J.; Wang, L.; Yang, M.; Zhu, Y.; Tomsia, A.; Mao, C. Untangling the Effects of Peptide Sequences and Nanotopographies in a Biomimetic Niche for Directed Differentiation of Ipscs by Assemblies of Genetically Engineered Viral Nanofibers. *Nano Lett.* **2014**, *14*, 6850−6856.

(17) Engler, A. J.; Sen, S.; Sweeney, H. L.; Discher, D. E. Matrix Elasticity Directs Stem Cell Lineage Specification. *Cell* **2006**, *126*, 677−689.

(18) Tejeda-Montes, E.; Smith, K. H.; Rebollo, E.; Gomez, R.; Alonso, M.; Rodriguez-Cabello, J. C.; Engel, E.; Mata, A. Bioactive Membranes for Bone Regeneration Applications: Effect of Physical and Biomolecular Signals on Mesenchymal Stem Cell Behavior. *Acta Biomater.* **2014**, *10*, 134−141.

(19) Kabosova, A.; Kramerov, A. A.; Aoki, A. M.; Murphy, G.; Zieske, J. D.; Ljubimov, A. V. Human Diabetic Corneas Preserve Wound Healing, Basement Membrane, Integrin and Mmp-10 Differences from Normal Corneas in Organ Culture. *Exp. Eye Res.* **2003**, *77*, 211−217.

(20) Bhatia, S. N.; Balis, U. J.; Yarmush, M. L.; Toner, M. Effect of Cell-Cell Interactions in Preservation of Cellular Phenotype: Cocultivation of Hepatocytes and Nonparenchymal Cells. *FASEB J.* **1999**, *13*, 1883−1900.

(21) Oh, S.; Brammer, K. S.; Li, Y. S.; Teng, D.; Engler, A. J.; Chien, S.; Jin, S. Stem Cell Fate Dictated Solely by Altered Nanotube Dimension. *Proc. Natl. Acad. Sci. U. S. A.* **2009**, *106*, 2130−2135.

(22) Guilak, F.; Cohen, D. M.; Estes, B. T.; Gimble, J. M.; Liedtke, W.; Chen, C. S. Control of Stem Cell Fate by Physical Interactions with the Extracellular Matrix. *Cell Stem Cell* **2009**, *5*, 17−26.

(23) Dalby, M. J.; Gadegaard, N.; Tare, R.; Andar, A.; Riehle, M. O.; Herzyk, P.; Wilkinson, C. D.; Oreffo, R. O. The Control of Human Mesenchymal Cell Differentiation Using Nanoscale Symmetry and Disorder. *Nat. Mater.* **2007**, *6*, 997−1003.

(24) Biggs, M. J.; Richards, R. G.; Gadegaard, N.; Wilkinson, C. D.; Oreffo, R. O.; Dalby, M. J. The Use of Nanoscale Topography to Modulate the Dynamics of Adhesion Formation in Primary Osteoblasts and Erk/Mapk Signalling in Stro-1+ Enriched Skeletal Stem Cells. *Biomaterials* **2009**, *30*, 5094−5103.

(25) Cassidy, J. W.; Roberts, J. N.; Smith, C. A.; Robertson, M.; White, K.; Biggs, M. J.; Oreffo, R. O.; Dalby, M. J. Osteogenic Lineage Restriction by Osteoprogenitors Cultured on Nanometric Grooved Surfaces: The Role of Focal Adhesion Maturation. *Acta Biomater.* **2014**, *10*, 651−660.

(26) Fayaz, H. C.; Giannoudis, P. V.; Vrahas, M. S.; Smith, R. M.; Moran, C.; Pape, H. C.; Krettek, C.; Jupiter, J. B. The Role of Stem Cells in Fracture Healing and Nonunion. *Int. Orthop.* **2011**, *35*, 1587−1597.

(27) Hannouche, D. P. H; Sedel, L. Current Trends in the Enhancement of Fracture Healing. *J. Bone Jt. Surg., Br. Vol.* **2001**, *83*, 157−164.

(28) Einhorn, T. A. The Science of Fracture Healing. *J. Orthop. Trauma.* **2005**, *19*, S4−S6.

(29) Claes, L.; Recknagel, S.; Ignatius, A. Fracture Healing under Healthy and Inflammatory Conditions. *Nat. Rev. Rheumatol.* **2012**, *8*, 133−143.

(30) Augustin, G.; Antabak, A.; Davila, S. The Periosteum. Part 1: Anatomy, Histology and Molecular Biology. *Injury* **2007**, *38*, 1115−1130.

(31) Rezwan, K.; Chen, Q. Z.; Blaker, J. J.; Boccaccini, A. R. Biodegradable and Bioactive Porous Polymer/Inorganic Composite Scaffolds for Bone Tissue Engineering. *Biomaterials* **2006**, *27*, 3413−3431.

(32) Habibovic, P.; Barralet, J. E. Bioinorganics and Biomaterials: Bone Repair. *Acta Biomater.* **2011**, *7*, 3013−3026.

(33) Huang, C.; Fu, X.; Liu, J.; Qi, Y.; Li, S.; Wang, H. The Involvement of Integrin B1 Signaling in the Migration and Myofibroblastic Differentiation of Skin Fibroblasts on Anisotropic Collagen-Containing Nanofibers. *Biomaterials* **2012**, *33*, 1791−1800.

(34) Marsell, R.; Einhorn, T. A. The Biology of Fracture Healing. *Injury* **2011**, *42*, 551−555.

(35) Shi, X.; Chen, S.; Zhao, Y.; Lai, C.; Wu, H. Enhanced Osteogenesis by a Biomimic Pseudo-Periosteum-Involved Tissue Engineering Strategy. *Adv. Healthcare Mater.* **2013**, *2*, 1229−1235.

DOI: 10.1021/acsami.5b07976
ACS Appl. Mater. Interfaces 2015, 7, 23336−23345

(36) Shi, X.; Fujie, T.; Saito, A.; Takeoka, S.; Hou, Y.; Shu, Y.; Chen, M.; Wu, H.; Khademhosseini, A. Periosteum-Mimetic Structures Made from Freestanding Microgrooved Nanosheets. *Adv. Mater.* **2014**, *26*, 3290−3296.
(37) You, M.-H.; Kwak, M. K.; Kim, D.-H.; Kim, K.; Levchenko, A.; Kim, D.-Y.; Suh, K.-Y. Synergistically Enhanced Osteogenic Differentiation of Human Mesenchymal Stem Cells by Culture on Nanostructured Surfaces with Induction Media. *Biomacromolecules* **2010**, *11*, 1856−1862.
(38) Woodruff, M. A.; Hutmacher, D. W. The Return of a Forgotten Polymer—Polycaprolactone in the 21st Century. *Prog. Polym. Sci.* **2010**, *35*, 1217−1256.
(39) Williams, J. M.; Adewunmi, A.; Schek, R. M.; Flanagan, C. L.; Krebsbach, P. H.; Feinberg, S. E.; Hollister, S. J.; Das, S. Bone Tissue Engineering Using Polycaprolactone Scaffolds Fabricated Via Selective Laser Sintering. *Biomaterials* **2005**, *26*, 4817−4827.
(40) Augat, P.; Simon, U.; Liedert, A.; Claes, L. Mechanics and Mechano-Biology of Fracture Healing in Normal and Osteoporotic Bone. *Osteoporosis Int.* **2005**, *16* (Suppl 2), S36−S43.
(41) Marsh, D. R.; Li, G. The Biology of Fracture Healing: Optimising Outcome. *Br. Med. Bull.* **1999**, *55*, 856−869.
(42) Pattanayak, D. K.; Rao, B. T.; Mohan, T. R. R. Calcium Phosphate Bioceramics and Bioceramic Composites. *J. Sol-Gel Sci. Technol.* **2011**, *59*, 432−447.
(43) Rosset, P.; Deschaseaux, F.; Layrolle, P. Cell Therapy for Bone Repair. *Orthop. Traumatol Surg. Res.* **2014**, *100*, S107−S112.
(44) Calori, G. M.; Giannoudis, P. V. Enhancement of Fracture Healing with the Diamond Concept: The Role of the Biological Chamber. *Injury* **2011**, *42*, 1191−1193.
(45) Puleo, D. A.; Nanci, A. Understanding and Controlling the Bone-Implant Interface. *Biomaterials* **1999**, *20*, 2311−2321.
(46) Habibovic, P.; de Groot, K. Osteoinductive Biomaterials - Properties and Relevance in Bone Repair. *J. Tissue Eng. Regener. Med.* **2007**, *1*, 25−32.
(47) Yim, E. K. F.; Darling, E. M.; Kulangara, K.; Guilak, F.; Leong, K. W. Nanotopography-Induced Changes in Focal Adhesions, Cytoskeletal Organization, and Mechanical Properties of Human Mesenchymal Stem Cells. *Biomaterials* **2010**, *31*, 1299−1306.
(48) Tawfick, S.; De Volder, M.; Copic, D.; Park, S. J.; Oliver, C. R.; Polsen, E. S.; Roberts, M. J.; Hart, A. J. Engineering of Micro- and Nanostructured Surfaces with Anisotropic Geometries and Properties. *Adv. Mater.* **2012**, *24*, 1628−1674.
(49) Klymov, A.; Prodanov, L.; Lamers, E.; Jansen, J. A.; Walboomers, X. F. Understanding the Role of Nano-Topography on the Surface of a Bone-Implant. *Biomater. Sci.* **2013**, *1*, 135.
(50) Londono, C.; Loureiro, M. J.; Slater, B.; Lucker, P. B.; Soleas, J.; Sathananthan, S.; Aitchison, J. S.; Kabla, A. J.; McGuigan, A. P. Nonautonomous Contact Guidance Signaling During Collective Cell Migration. *Proc. Natl. Acad. Sci. U. S. A.* **2014**, *111*, 1807−1812.
(51) Huang, C.; Fu, X.; Liu, J.; Qi, Y.; Li, S.; Wang, H. The Involvement of Integrin Beta1 Signaling in the Migration and Myofibroblastic Differentiation of Skin Fibroblasts on Anisotropic Collagen-Containing Nanofibers. *Biomaterials* **2012**, *33*, 1791−1800.
(52) Sprague, E. A.; Tio, F.; Ahmed, S. H.; Granada, J. F.; Bailey, S. R. Impact of Parallel Micro-Engineered Stent Grooves on Endothelial Cell Migration, Proliferation, and Function: An in Vivo Correlation Study of the Healing Response in the Coronary Swine Model. *Circ.: Cardiovasc. Interventions* **2012**, *5*, 499−507.
(53) Palmaz, J. C.; Benson, A.; Sprague, E. A. Influence of Surface Topography on Endothelialization of Intravascular Metallic Material. *J. Vasc. Interv. Radiol.* **1999**, *10*, 439−444.
(54) Evans, M. D.; McFarland, G. A.; Taylor, S.; Walboomers, X. F. The Response of Healing Corneal Epithelium to Grooved Polymer Surfaces. *Biomaterials* **2005**, *26*, 1703−1711.
(55) Tay, C. Y.; Cai, P.; Setyawati, M. I.; Fang, W.; Tan, L. P.; Hong, C. H.; Chen, X.; Leong, D. T. Nanoparticles Strengthen Intracellular Tension and Retard Cellular Migration. *Nano Lett.* **2014**, *14*, 83−88.
(56) Leong, D. T.; Abraham, M. C.; Rath, S. N.; Lim, T. C.; Chew, F. T.; Hutmacher, D. W. Investigating the Effects of Preinduction on Human Adipose-Derived Precursor Cells in an Athymic Rat Model. *Differentiation (Oxford, U. K.)* **2006**, *74*, 519−529.
(57) Leong, D. T.; Khor, W. M.; Chew, F. T.; Lim, T.-C.; Hutmacher, D. W. Characterization of Osteogenically Induced Adipose Tissue-Derived Precursor Cells in 2-Dimensional and 3-Dimensional Environments. *Cells Tissues Organs* **2006**, *182*, 1−11.
(58) Oh, S.; Brammer, K. S.; Li, Y. S.; Teng, D.; Engler, A. J.; Chien, S.; Jin, S. Stem Cell Fate Dictated Solely by Altered Nanotube Dimension. *Proc. Natl. Acad. Sci. U. S. A.* **2009**, *106*, 2130−2135.
(59) Provenzano, P. P.; Inman, D. R.; Eliceiri, K. W.; Trier, S. M.; Keely, P. J. Contact Guidance Mediated Three-Dimensional Cell Migration Is Regulated by Rho/Rock-Dependent Matrix Reorganization. *Biophys. J.* **2008**, *95*, 5374−5384.
(60) Yang, Y.; Kusano, K.; Frei, H.; Rossi, F.; Brunette, D. M.; Putnins, E. E. Microtopographical Regulation of Adult Bone Marrow Progenitor Cells Chondrogenic and Osteogenic Gene and Protein Expressions. *J. Biomed. Mater. Res., Part A* **2010**, *95*, 294−304.
(61) Weiner, S.; Wagner, H. D. The Material Bone: Structure-Mechanical Function Relations. *Annu. Rev. Mater. Sci.* **1998**, *28*, 271−298.

DOI: 10.1021/acsami.5b07976
ACS Appl. Mater. Interfaces 2015, 7, 23336−23345